Electronic Supplementary Information

Relaxation processes in a single crystal of $Co(NCS)_2$(4-methoxypyridine)$_2$ spin chain

Magdalena Foltyn[a]*, Dawid Pinkowicz[b], Christian Näther[c], Michał Rams[a]

[a] *Institute of Physics, Jagiellonian University, Łojasiewicza 11, 30348 Kraków, Poland. E-mail: magdalena.foltyn@uj.edu.pl*;
[b] *Faculty of Chemistry, Jagiellonian University, Gronostajowa 2, 30-387 Kraków, Poland*;
[c] *Institut für Anorganische Chemie, Christian-Albrechts-Universität zu Kiel, Max-Eyth-Straße 2, 24118 Kiel, Germany*;

1-sc – single crystal sample of $[Co(NCS)_2(4\text{-methoxypyridine})_2]_n$
1-p – previously investigated powder sample of $[Co(NCS)_2(4\text{-methoxypyridine})_2]_n$
1-g1 – powder sample of $[Co(NCS)_2(4\text{-methoxypyridine})_2]_n$ obtained by grounding crystals
1-g2 – powder sample of $[Co(NCS)_2(4\text{-methoxypyridine})_2]_n$ obtained by grounding crystals twice

Synthesis and Crystallographic studies

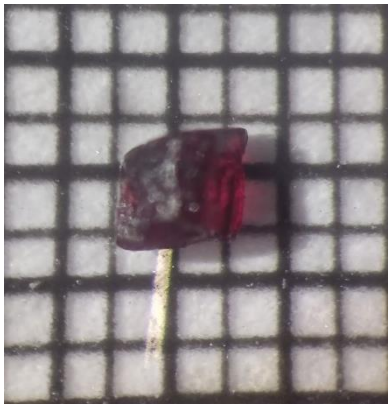

Figure S1. A photo of the single crystal of **1-sc** that was used for magnetic investigations. The smallest grid is 0.5 mm.

Tab. S1. Selected crystallographic data for **1-sc**.

Space group	$P\bar{1}$
a [Å]	8.9577(5)
b [Å]	10.3859(7)
c [Å]	10.8543(7)
α [°]	66.188(2)
β [°]	67.991(2)
γ [°]	82.987(2)
Z	2
T [K]	296

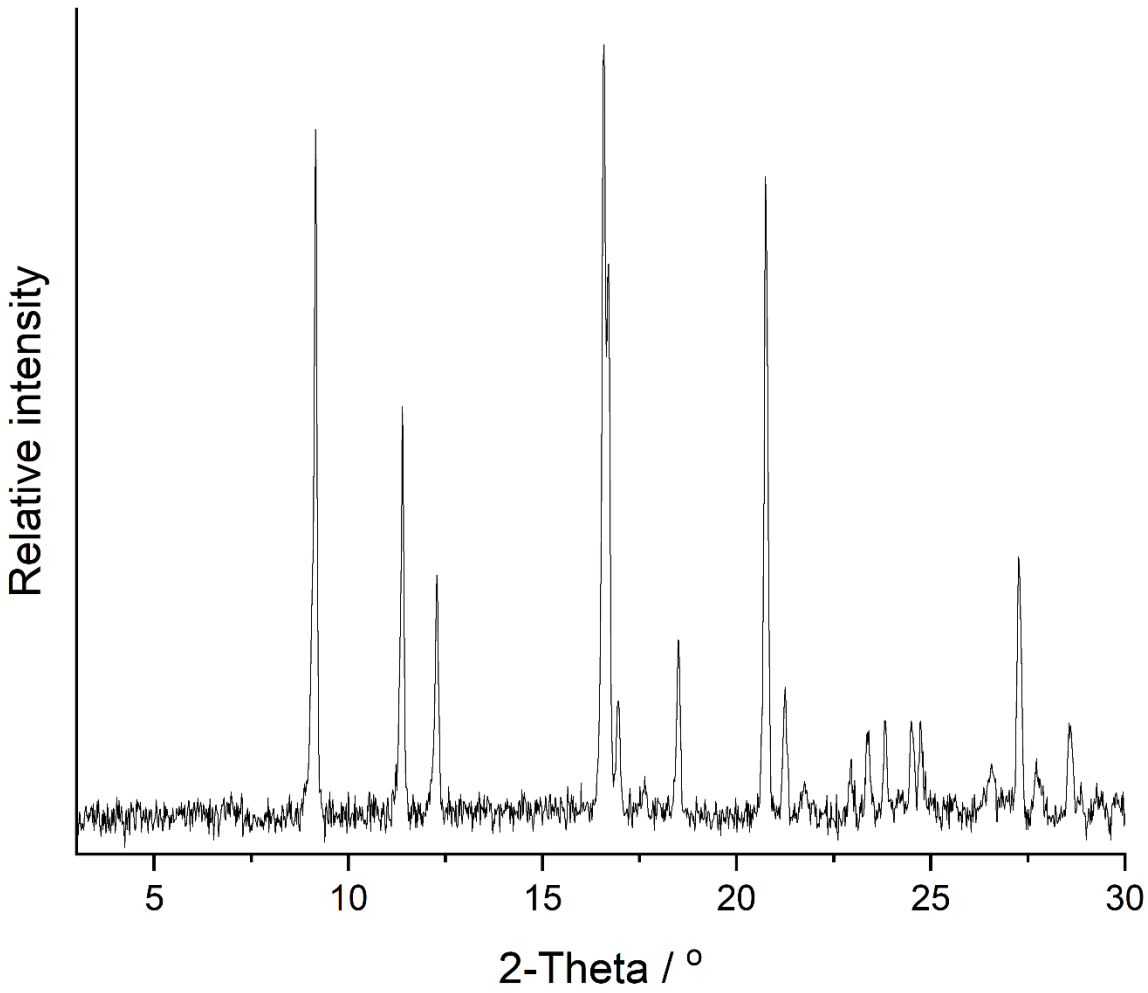

Figure S2. Experimental PXRD pattern for **1-sc**. The pattern is the same as the experimental and theoretical patterns published in [1] (Fig. S2 in [1], patterns A and B, Supporting Information). No other phases are present, confirming the purity of the sample.

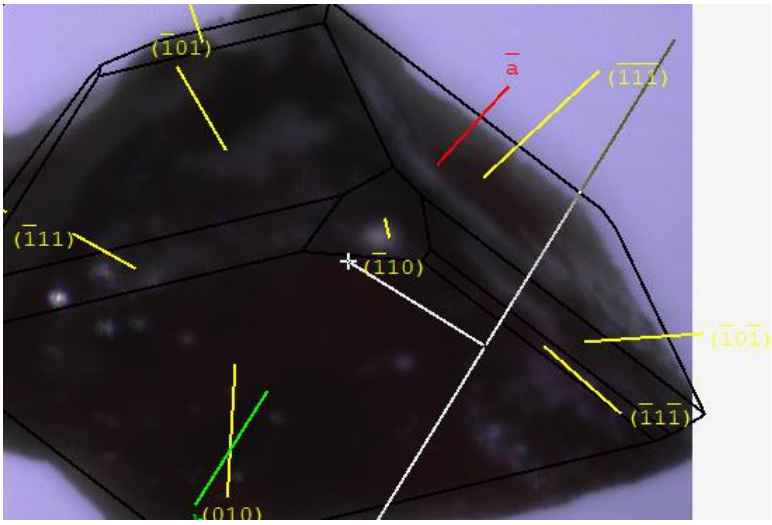

Figure S3. The photo of the single crystal of **1**, with the faces indexed.

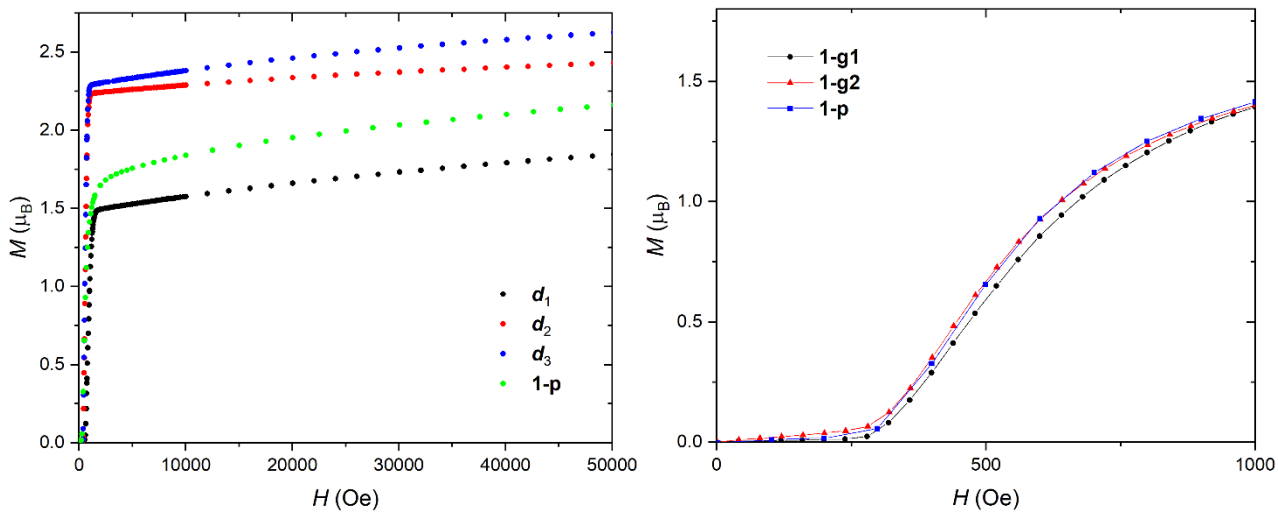

Figure S4. Left: Magnetization curves measured along 3 perpendicular directions of a single crystal sample, **1-sc**, at 1.8 K presented up to 50 kOe. Right: The magnetization curves for powder samples. Blue points: data already published in [1].

Experimental determination of the direction of the easy axis

$\boldsymbol{d}_1$ is ⊥ to the (010) plane, $\boldsymbol{d}_2$ =[100], $\boldsymbol{d}_3 = \boldsymbol{d}_1 \times \boldsymbol{d}_2$. Vectors $\boldsymbol{d}_1$, $\boldsymbol{d}_2$, $\boldsymbol{d}_3$ are normalized to 1.

The experimental magnetization easy axis, $\boldsymbol{M}_{\mathrm{ea}}$, was calculated by solving 3 equations of projections of $\boldsymbol{M}_{\mathrm{ea}}$ on the directions of the measurement:

$$M_1 = |\boldsymbol{M}_{\mathrm{ea}} \cdot \boldsymbol{d}_1| \qquad M_2 = |\boldsymbol{M}_{\mathrm{ea}} \cdot \boldsymbol{d}_2| \qquad M_3 = |\boldsymbol{M}_{\mathrm{ea}} \cdot \boldsymbol{d}_3|$$

The results are: $\boldsymbol{M}_{ea}$ = (2.22, −0.44, 2.65) μ_B.

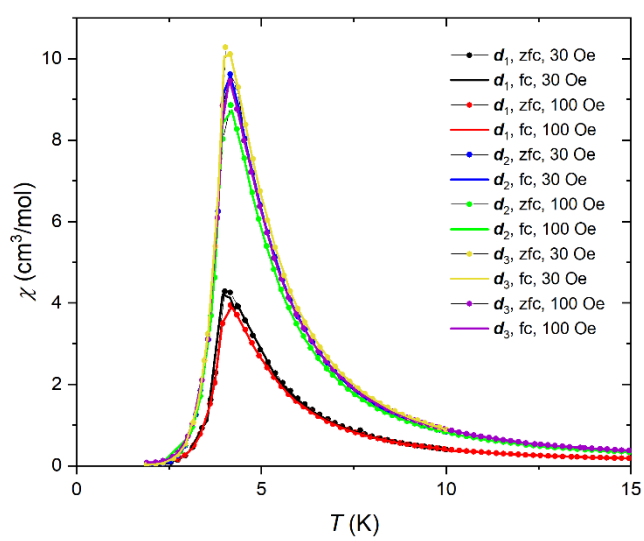

Figure S5. Zero-field cooled and field cooled susceptibility measured for **1-sc** along 3 perpendicular directions of a single crystal sample at 30 and 100 Oe.

Equations used to simultaneously fit magnetic susceptibility measured along 3 perpendicular directions of single crystal sample of 1

Coordinate system (x, y, z) corresponds to the main axes of susceptibility tensor that is diagonal in this system. The z direction is the easy axis direction of magnetization. The measurements were done in 3 perpendicular directions denoted as $(\mathbf{d}_1, \mathbf{d}_2, \mathbf{d}_3)$, that create another coordinate system. The rotation matrix $\mathbf{R}$ between these two systems can be parametrized by proper Euler angles $(\alpha_1, \alpha_2, \alpha_3)$

$$\mathbf{R} = \begin{pmatrix} \cos\alpha_1\cos\alpha_3 - \cos\alpha_2\sin\alpha_1\sin\alpha_3 & -\cos\alpha_1\sin\alpha_3 - \cos\alpha_2\cos\alpha_3\sin\alpha_1 & \sin\alpha_1\sin\alpha_2 \\ \cos\alpha_3\sin\alpha_1 + \cos\alpha_1\cos\alpha_2\sin\alpha_3 & \cos\alpha_1\cos\alpha_2\cos\alpha_3 - \sin\alpha_1\sin\alpha_3 & -\cos\alpha_1\sin\alpha_2 \\ \sin\alpha_2\sin\alpha_3 & \cos\alpha_3\sin\alpha_2 & \cos\alpha_2 \end{pmatrix}$$

The magnetization in the ordered state $(M_x = 0, M_y = 0, M_z = M_{ea})$ transforms as

$$\begin{pmatrix} M_1 \\ M_2 \\ M_3 \end{pmatrix} = \mathbf{R} \begin{pmatrix} 0 \\ 0 \\ M_{ea} \end{pmatrix}$$

Using experimental values of (M_1, M_2, M_3) it is possible to calculate the angles α_1 and α_2.

$$\tan\alpha_1 = -M_1/M_2$$

$$\tan\alpha_2 = \sqrt{M_{ea}^2 - M_3^2}/M_3$$

The angle α_3 that determines the rotation of (x, y) axes around z axis cannot be determined using only data in the ordered phase, therefore α_3 remains a free parameter during fitting the susceptibility in the paramagnetic state. Magnetic susceptibility tensor

$$\chi_{xyz} = \begin{pmatrix} \chi_{xx} & 0 & 0 \\ 0 & \chi_{yy} & 0 \\ 0 & 0 & \chi_{zz} \end{pmatrix},$$

which is a second order tensor, transforms as

$$\chi_{123} = \mathbf{R} \cdot \chi_{xyz} \cdot \mathbf{R}^T$$

and the diagonal elements of χ_{123} are the susceptibilities measured in $\mathbf{d}_1, \mathbf{d}_2, \mathbf{d}_3$ directions.

<u>The magnetic susceptibility tensor ($\chi_{xx}, \chi_{yy}, \chi_{zz}$)</u> was modeled using the Hamiltonian for Ising chain of spin s =1/2 (***H*** - magnetic field, J - intrachain interaction, $\hat{g}$ - g factor tensor):

$$\mathcal{H} = -J\sum_j s_j^z s_{j+1}^z + \mu_B \sum_j \boldsymbol{H} \cdot \hat{g} \cdot \boldsymbol{s}_j$$

The equations for magnetic susceptibility along x, y, z derived by Fischer[2]:

$$\chi_{xx}^{chain} = \frac{N_A \mu_B^2 g_x^2}{2J}\left[\tanh\left(\frac{J}{4k_BT}\right) + \frac{J}{4k_BT}\mathrm{sech}^2\left(\frac{J}{k_BT}\right)\right]$$

$$\chi_{yy}^{chain} = \frac{N_A \mu_B^2 g_y^2}{2J}\left[\tanh\left(\frac{J}{4k_BT}\right) + \frac{J}{4k_BT}\mathrm{sech}^2\left(\frac{J}{k_BT}\right)\right]$$

$$\chi_{zz}^{chain} = \frac{N_A \mu_B^2 g_z^2}{4k_BT}\exp\left(\frac{J}{2k_BT}\right)$$

Taking into account the interchain interaction, zJ', within the mean field approximation[3] (χ_0 – temperature independent susceptibility:

$$\chi_{ii} = \frac{\chi_{ii}^{chain}}{1 - \chi_{ii}^{chain}\dfrac{zJ'}{N_A g_i^2 \mu_B^2}} + \chi_0$$

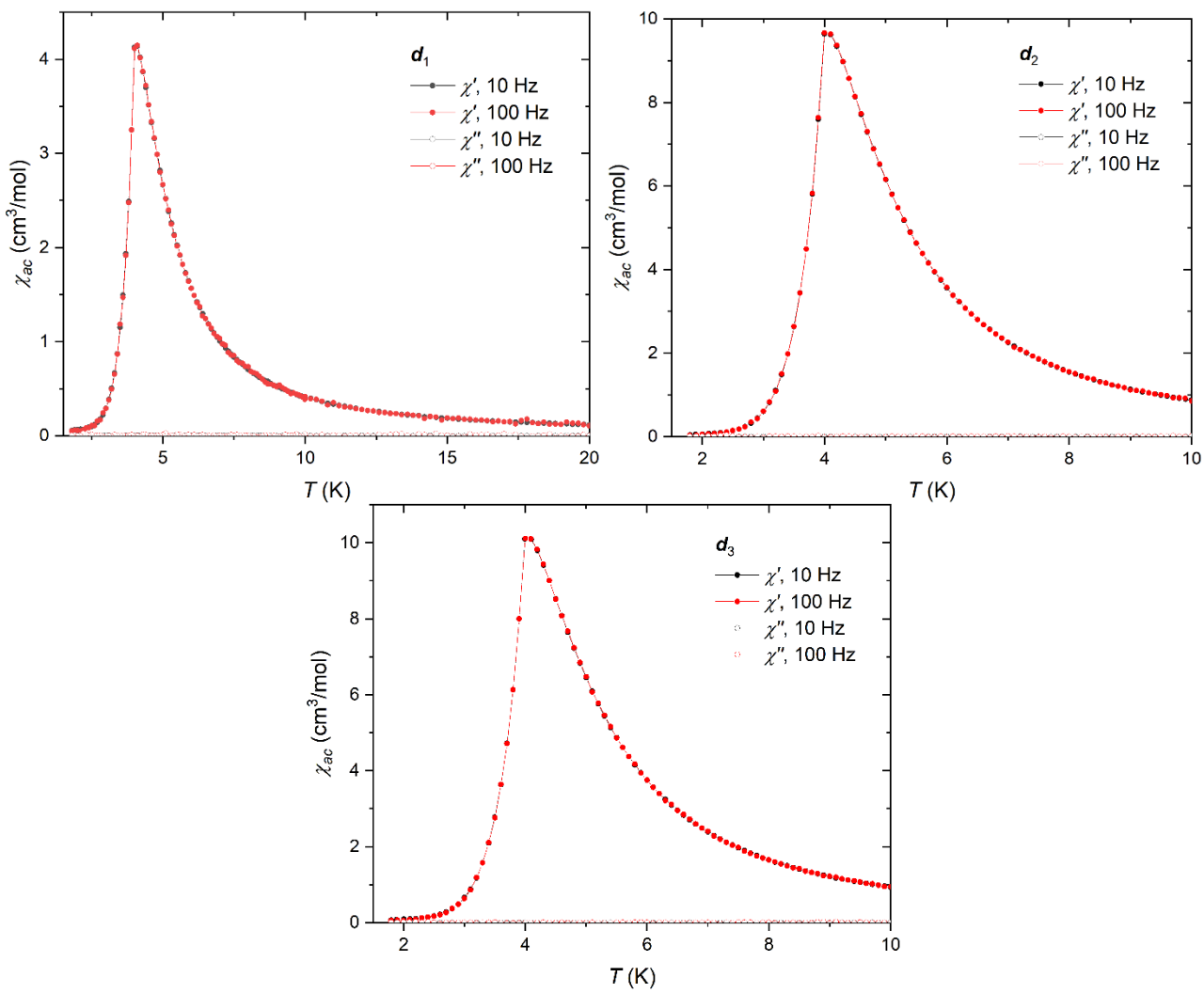

Figure S6. Ac magnetic susceptibility measured for **1-sc** at H_{dc} = 0 Oe, H_{ac} = 3 Oe along 3 perpendicular, crystallographic directions. The χ' data at 10 Hz were used in the analysis in Fig. S5.

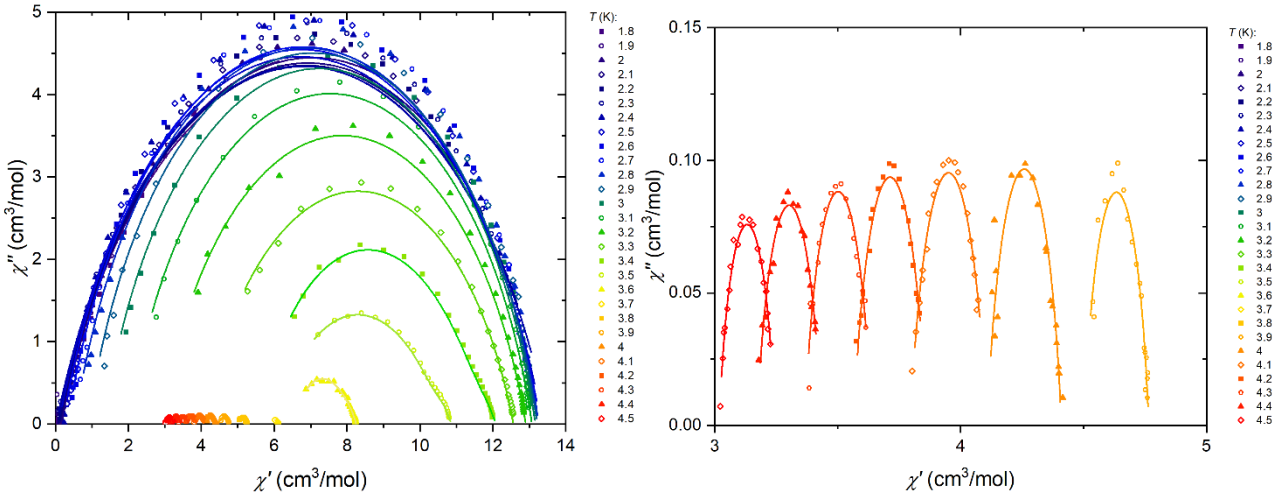

Figure S7. The Argand plots of ac magnetic susceptibility for **1-sc**, measured at H_{dc} = 800 Oe, H_{ac} = 3 Oe along $\boldsymbol{d}_1$ and analyzed using single-mode or double-mode Cole-Cole model. Left: all curves, right: enlarged curves for the highest temperatures.

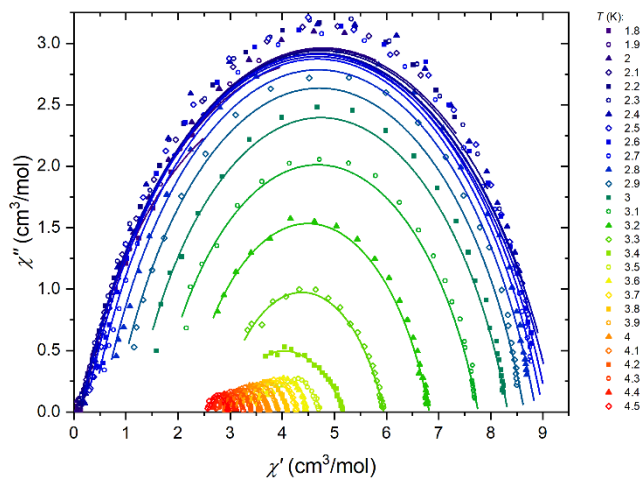

Figure S8. The Argand plots of ac magnetic susceptibility for **1-sc**, measured at H_{dc} = 1100 Oe, H_{ac} = 3 Oe along $\boldsymbol{d}_1$ and analyzed using single-mode or double-mode Cole-Cole model.

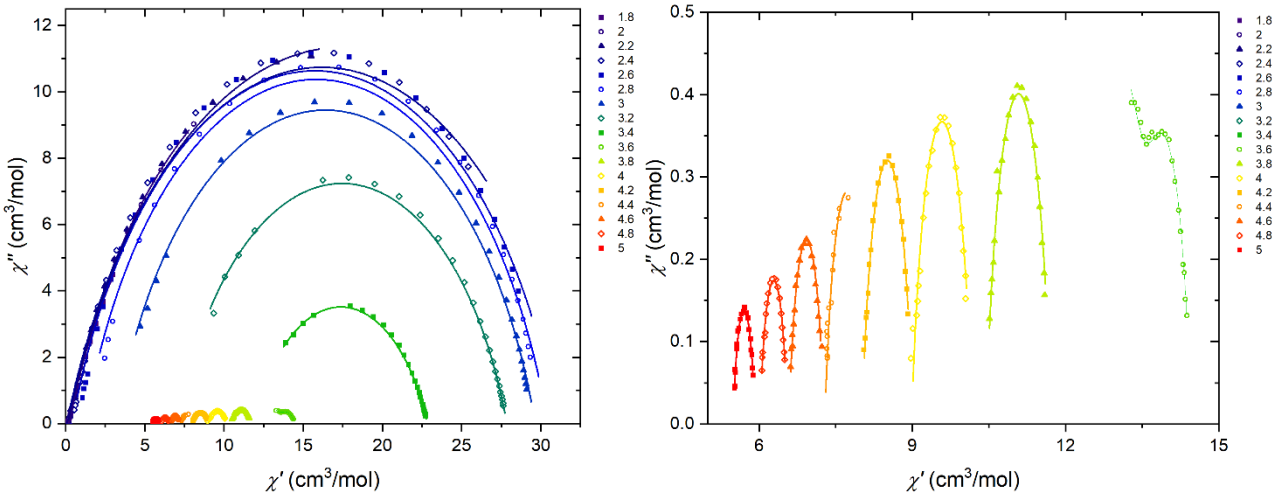

Figure S9. The Argand plots of ac magnetic susceptibility for **1-sc**, measured at H_{dc} = 600 Oe, H_{ac} = 3 Oe along $\boldsymbol{d}_1$ and analyzed using single-mode or double-mode Cole-Cole model. Left: all curves, right: enlarged curves for the highest temperatures.

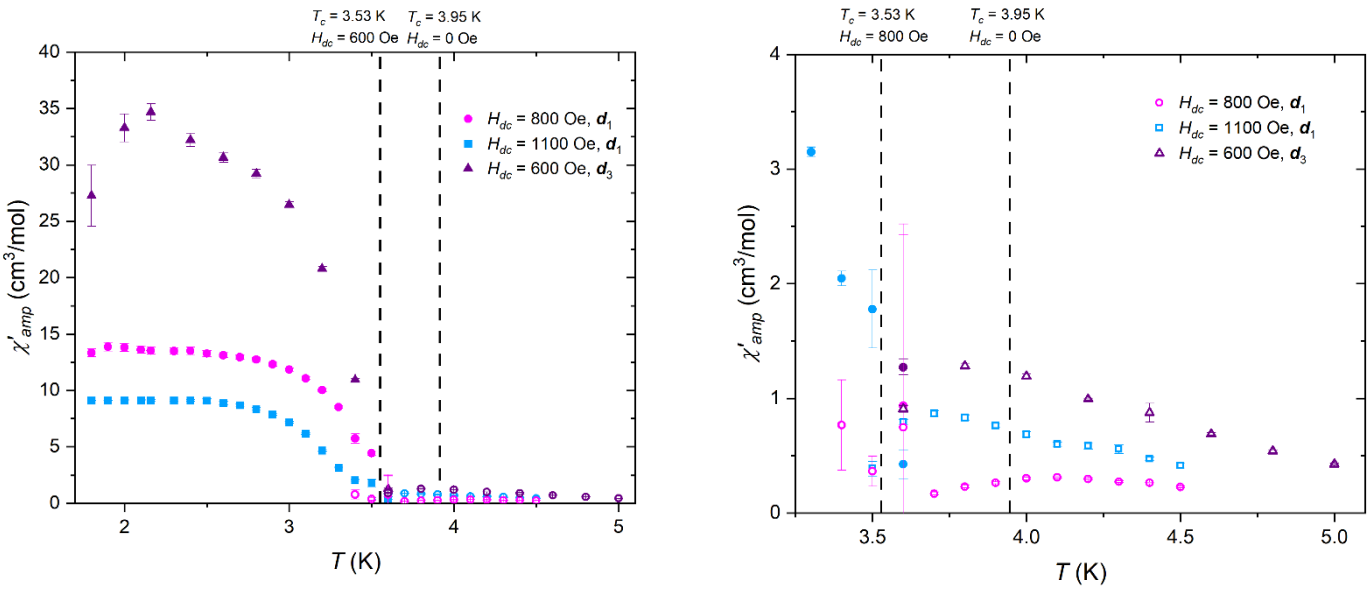

Figure S10. The temperature dependence of amplitudes determined from Cole-Cole model for all 3 measurements. Left: all temperatures. Right: Enlargement of the high-temperature region.

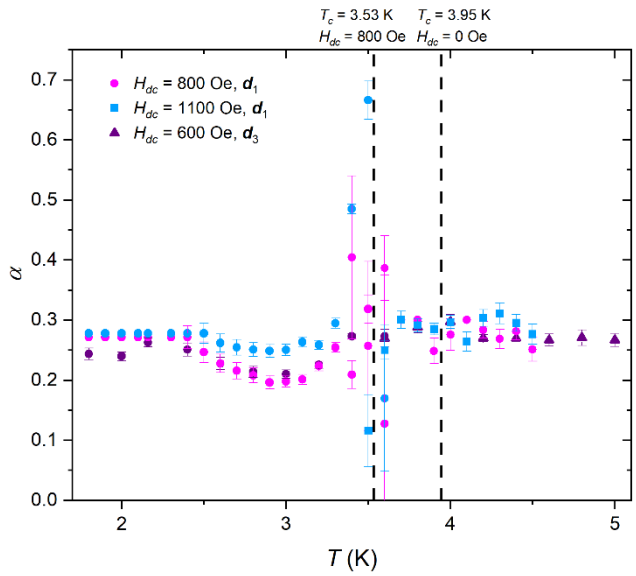

Figure S11. The α parameters determined from Cole-Cole model for all 3 measurements. The values at the lowest temperatures for measurements along $\boldsymbol{d}_1$ were fixed.

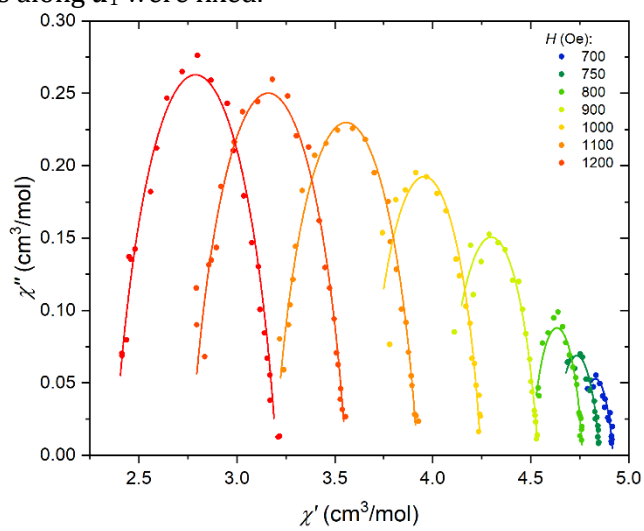

Figure S12. The Argand plot of the ac magnetic susceptibility for **1-sc**, measured at T = 3.9 K, H_{ac} = 3 Oe along $\boldsymbol{d}_1$ and analyzed using single-mode Cole-Cole model.

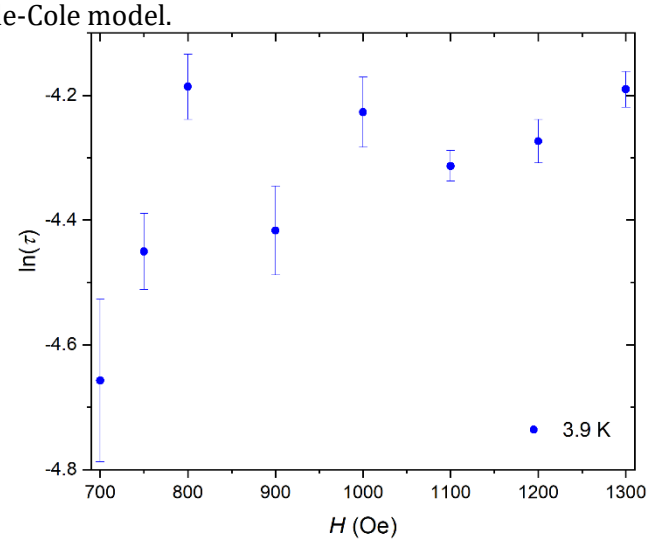

Figure S13. Field dependence of the relaxation time for a single crystal determined from fitting the Cole-Cole model for the measurement along $\boldsymbol{d}_1$ at 3.9 K.

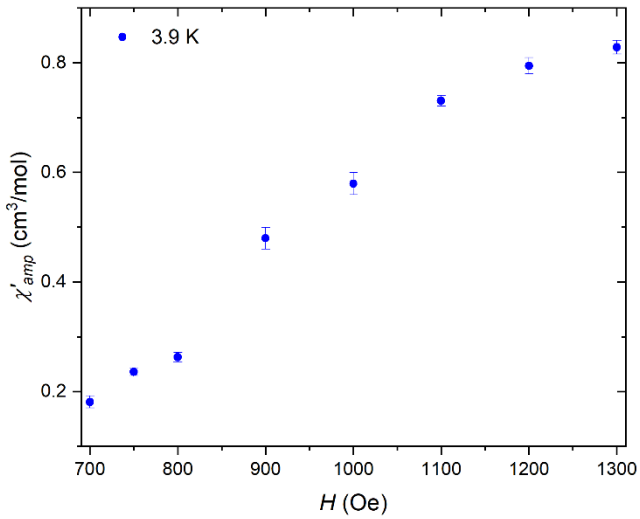

Figure S14. The field dependence of amplitudes determined from fitting the Cole-Cole model for the measurement along $\boldsymbol{d}_1$ at 3.9 K.

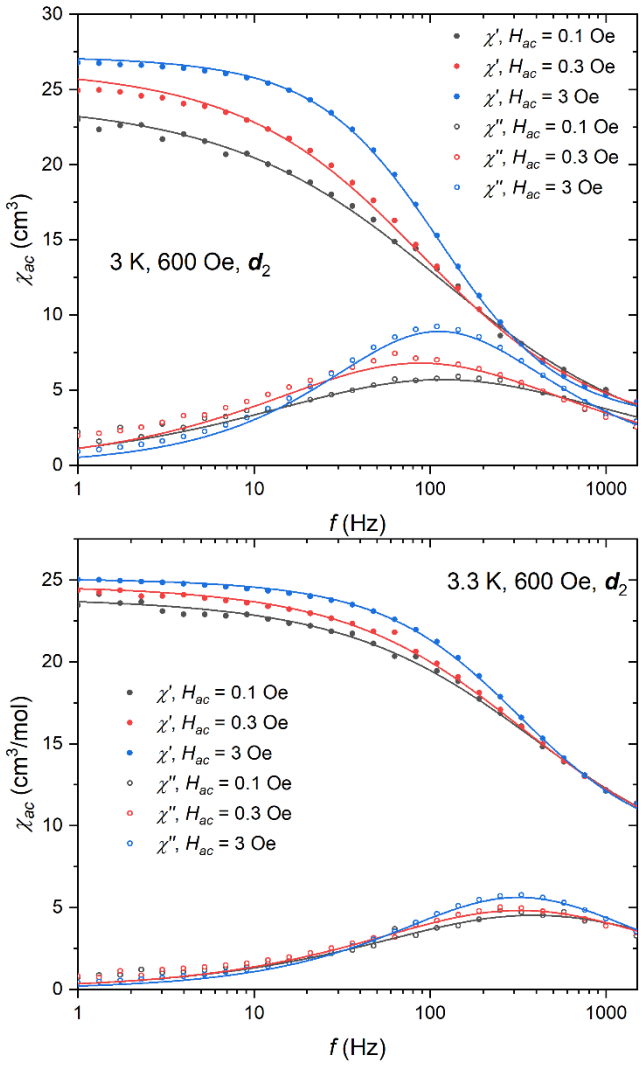

Figure S15. The ac magnetic susceptibility for **1-sc**, measured at T = 3.0 (top) and 3.3 K (bottom), H_{ac} = 3 Oe, H_{dc} = 600 Oe, along $\boldsymbol{d}_2$ direction and analyzed using the single-mode Cole-Cole model. No significant change of the position of the peak in χ'' is observed, which excludes the presence of the phonon bottleneck effect.

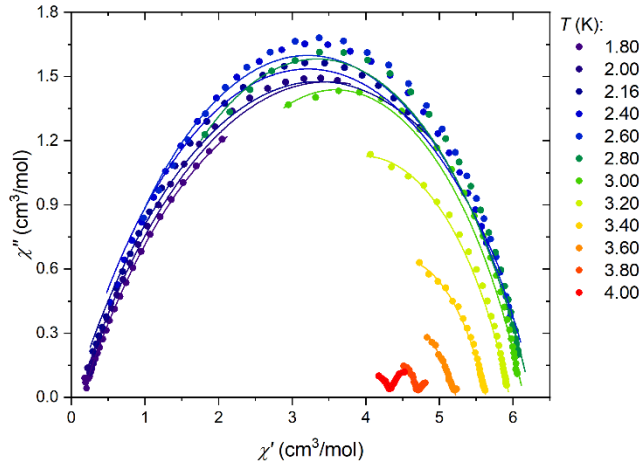

Figure S16. The Argand plot of the ac magnetic susceptibility measured at H_{dc} = 800 Oe, H_{ac} = 3 Oe for a powder sample **1-g1** and analyzed using single-mode Cole-Cole model.

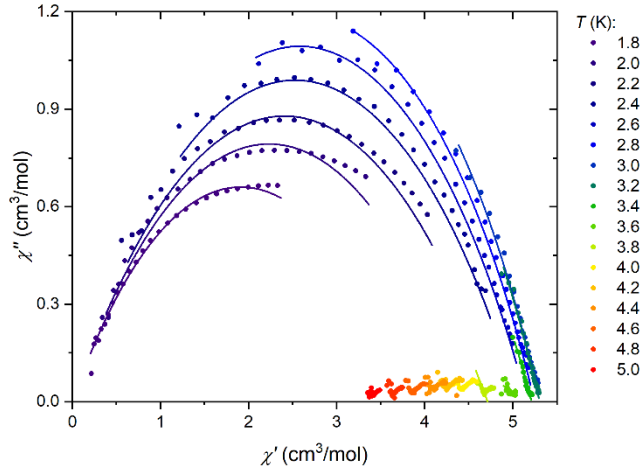

Figure S17. The Argand plot of the ac magnetic susceptibility measured at H_{dc} = 800 Oe, H_{ac} = 3 Oe for a powder sample **1-g2** and analyzed using single-mode Cole-Cole model.

Specific Heat Measurements

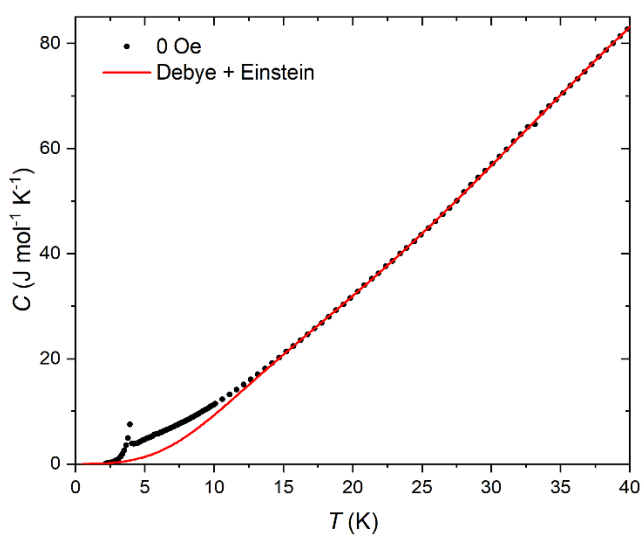

Figure S18. Temperature dependence of the specific heat of **1-sc** with the fit of a linear combination of Debye and Einstein model. The fit was performed for data in the range 20 – 40 K. Debye and Einstein temperatures are: θ_D =

72.4 (4.4) K, θ_E = 164.9 (5.1) K, the dimensionless amplitudes are: a_D = 2.11(16), a_E = 5.38(7). The parameters are in agreement with the values obtained for a powder sample: a_E=4.16(6), a_D=1.84(2), θ_D = 72.3(3) (4.4) K, θ_E = 150.3(2) K.[1]

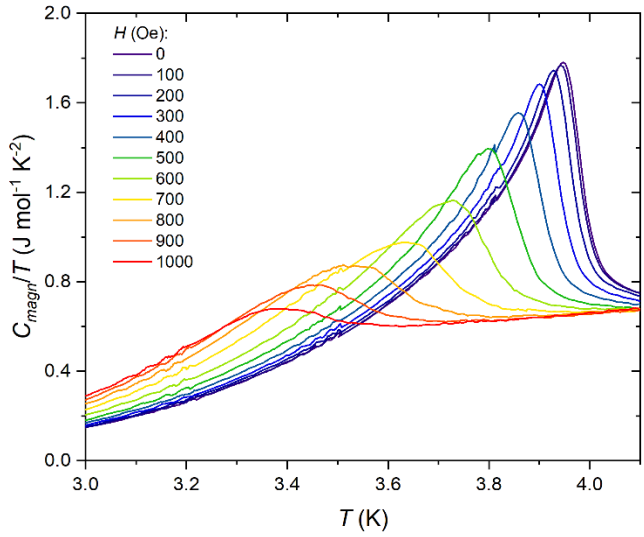

Figure S19. Temperature dependence of the magnetic contribution of specific heat for **1-sc**, C_{magn}, presented as C_{magn}/T, measured at different fields.

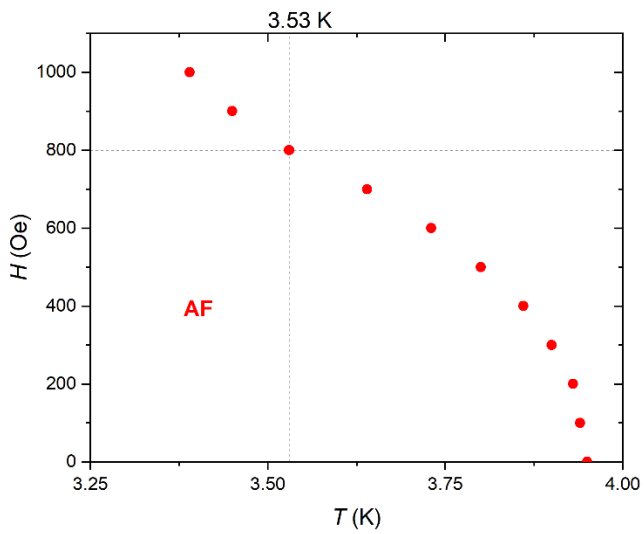

Figure S20. Magnetic phase diagram for **1-sc**. The points were determined as the $C_{magn}/T(T)$ maxima.

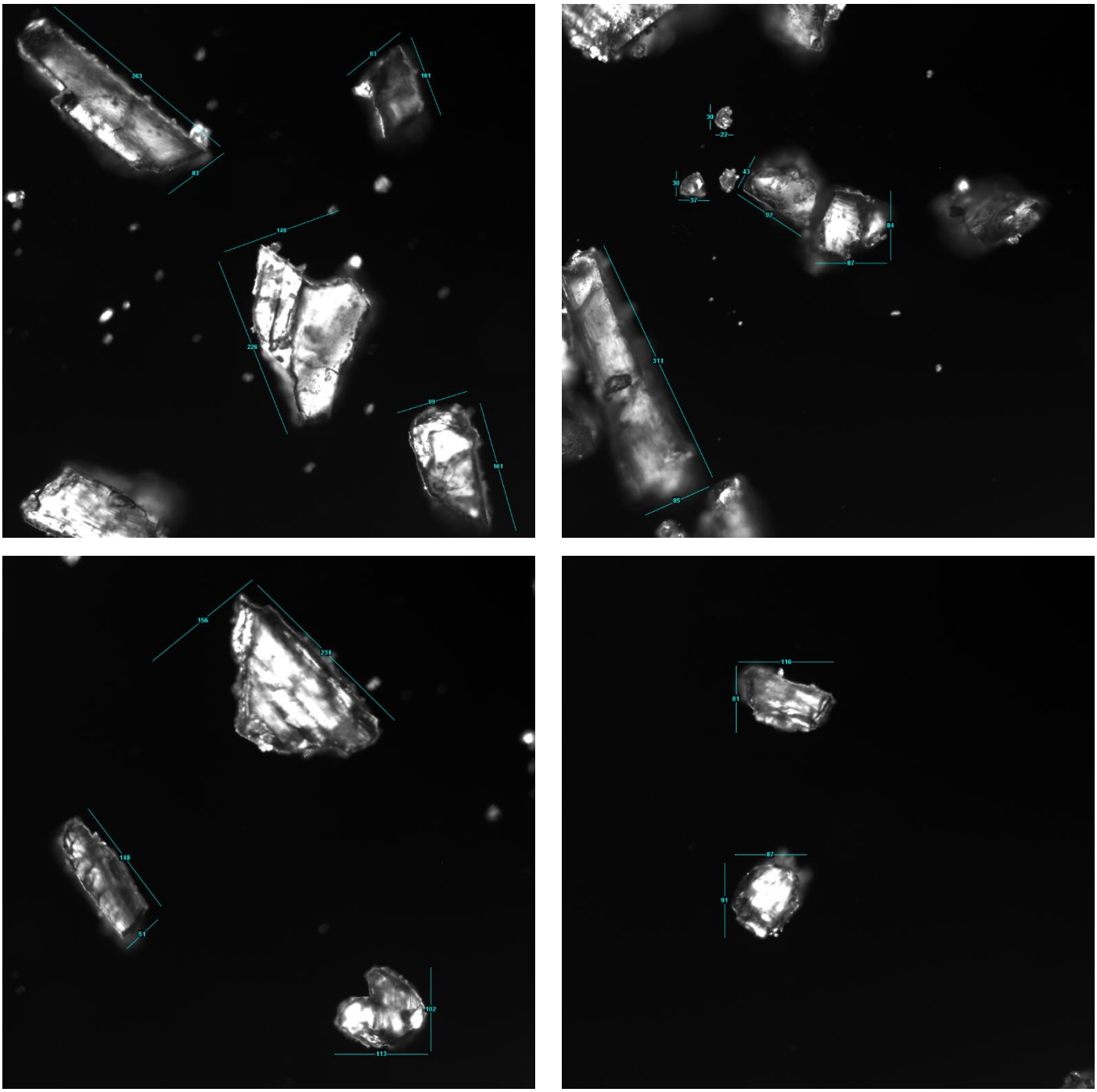

Fig. S21. The photo of crystallites in **1-g1** sample. Size of the photos: 648 μm × 648 μm. The blue lines are the measured distances, the blue numbers are their lengths in μm.

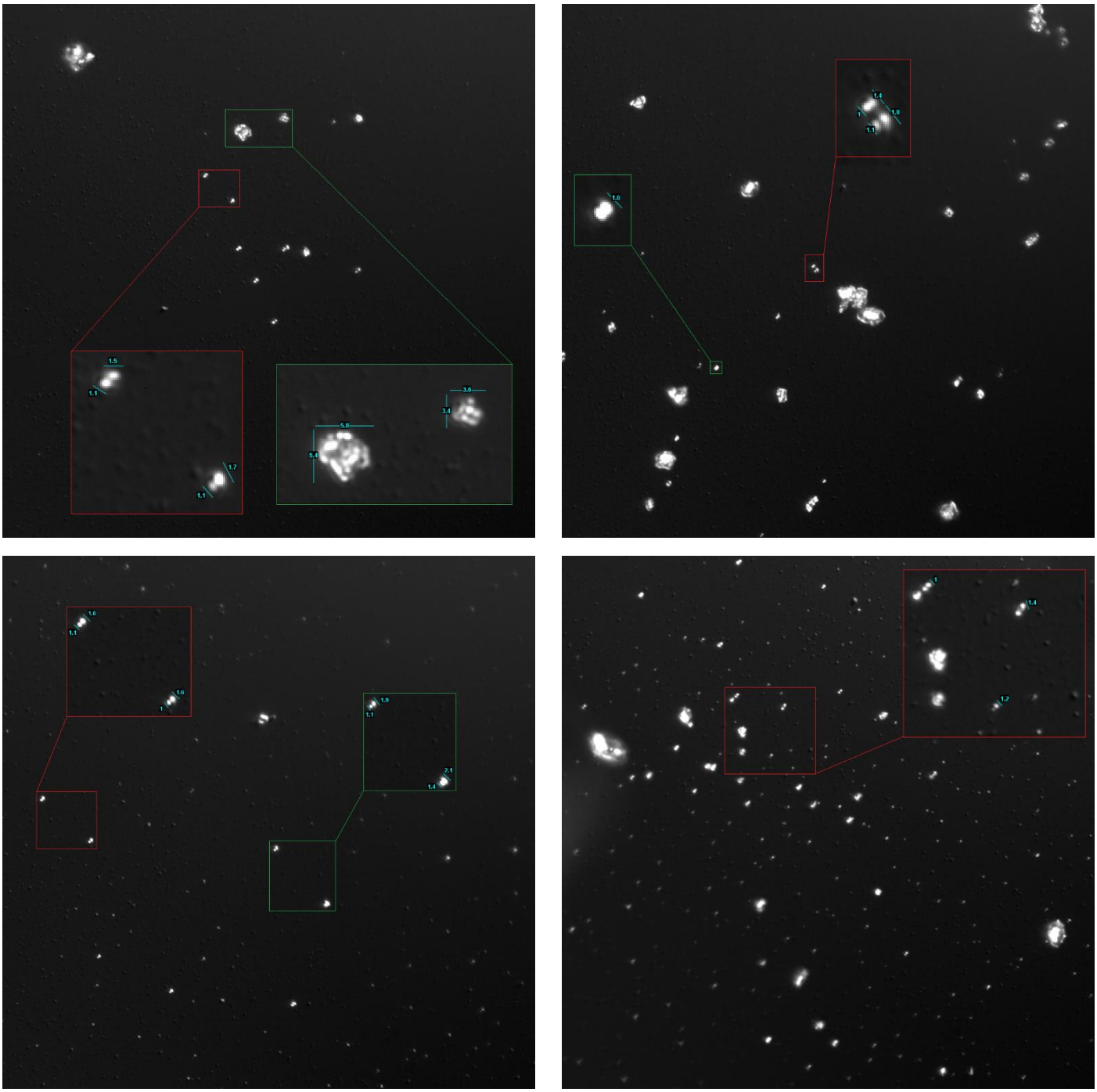

Fig. S22. The photo of crystallites in **1-g2** sample. Size of the photos: 161 μm × 161 μm. The blue lines are the measured distances, the blue numbers are their lengths in μm. With the smaller frames, there are marked the areas which are enlarged in larger frames.

References:

1. M. Rams, A. Jochim, M. Böhme, T. Lohmiller, M. Ceglarska, M. Rams, A. Schnegg, W. Plass and C. Näther, *Chemistry-a European Journal*, 2020, **26**, 2765-2765.
2. M. E. Fisher, *J Math Phys*, 1963, **4**, 124-135.
3. R. L. Carlin, *Magnetochemistry*, Springer-Verlag Berlin Heidelberg, 1986.